Application of SoleiTool for Density Estimation using CubeSat GPS Data

Shaylah Mutschler
University of Colorado Boulder
Penina Axelrad, Eric Sutton
University of Colorado Boulder, Space Weather Technology (SWx TREC)

ABSTRACT

A key requirement for accurate trajectory prediction and Space Domain Awareness (SDA) is knowledge of the non-conservative forces affecting space objects. These effects vary temporally and spatially and are primarily driven by the dynamical behavior of space weather. Existing SDA algorithms adjust space environment models based on observations of calibration satellites. Still, lack of sufficient data and mismodeling of non-conservative forces can cause inaccuracies in space object motion prediction. This work aims to improve our modeling of non-conservative forces, specifically atmospheric drag, by leveraging observations of objects not typically utilized for space environment monitoring.

Recently, there has been a rise in popularity of LEO CubeSats, with several companies establishing commercial CubeSat constellations for remote sensing and communication applications. Our research takes advantage of the abundance and quality of CubeSat GPS information to infer the space environment affecting their motion. We explore rigorous and practically realizable means to utilize CubeSats as indirect sensors of the space environment. The focus is on atmospheric density for more accurate prediction of LEO object motion.

In our previous work, we developed SoleiTool to estimate forcing parameters of a physics-based space environment model using debris tracking data. In this work, we expand SoleiTool's capabilities to estimate parameters of TIE-GCM using CubeSat GPS information. Precise Orbit Determination (POD) information from nine CubeSats over 11 days is used to sense a global density field when historical data shows two geomagnetic storms via elevated Kp values. This paper explores three SoleiTool approaches to estimate atmospheric density, and compares them to the operationally used model, as well as MSIS. We conclude with a suggestion for which approach is recommended moving forward.

1. INTRODUCTION

Our research explores rigorous and practically realizable means to utilize CubeSats as indirect sensors of the space environment. The focus is on atmospheric density for more accurate prediction of Low Earth Orbit (LEO) object motion. Current methods that estimate or model atmospheric density can be categorized as either empirical or physics-based approaches. Empirical models are computationally fast, but only represent the climatological atmospheric conditions. Physics-based models incorporate current knowledge of atmospheric conditions to provide forecasts, but require substantially more computing power than empirical models.

Recently, there has been a rapid rise in the number of deployed LEO CubeSats, with various commercial companies establishing CubeSat constellations for remote sensing and communication applications. Spire Global is in the process of deploying a 175-CubeSat constellation and currently operates a fleet of more than 100 LEO CubeSats. These CubeSats have onboard GPS receivers to provide accurate time and position estimates for operations. Our research takes advantage of the abundance and quality of CubeSat position information to infer the space environment affecting their motion. CubeSats are particularly well suited for this application due to their simple physical geometry, which is one to several 10x10x10 cm units (Spire CubeSats are 3U).

In our previous work, we developed SoleiTool to estimate forcing parameters of a physics-based space environment model, using debris tracking data [7]. Here, we expand SoleiTool's capabilities to estimate parameters of the Thermosphere-Ionosphere-Electrodynamics General Circulation Model (TIE-GCM) using CubeSat GPS Precise Orbit Determination (POD) data. We review the overall SoleiTool method in Section 2, before turning the attention to the

focus of this paper: exploring and evaluating several approaches for the SoleiTool second filter, the Particle Filter (PF). We analyze the performance of SoleiTool when applied to a case study spanning 11 days in May 2019. The global density field is sensed via the POD measurements from nine CubeSats during two geomagnetic storms (as shown via elevated historical Kp values in Fig. 3). We compare the density field estimated via three SoleiTool PF approaches during this case study and compare it with HASDM (used operationally) and MSIS [9] density.

Overall, our tool is expected to improve atmospheric density estimates by assimilating CubeSat GPS information to infer drivers to a physics-based space environment model, and will therefore allow for more accurate LEO object motion prediction. In doing so, we hope to decrease the number of unnecessary satellite maneuvers executed to avoid debris objects. This not only extends satellite lifetime, but also provides for a safer space environment by preserving fuel to mitigate actual collision risks.

1.1 Atmospheric Drag

An object in LEO experiences atmospheric drag caused by particles in the atmosphere colliding with the surface of the object. Drag acts primarily in the opposite direction of the velocity vector and effectively dissipates orbit energy. The magnitude of the force due to drag is directly dependent on neutral density (number of particles in the atmosphere). This is generally modeled in the equation of acceleration due to drag,

$$a_{drag} = -\frac{1}{2}\rho\frac{C_D A}{m}v_{rel}^2\frac{\vec{v}_{rel}}{|\vec{v}_{rel}|} \tag{1}$$

where

$$\vec{v}_{rel} = \frac{d\vec{r}}{dt} - \vec{\omega}_{\oplus}\times\vec{r} \tag{2}$$

is the velocity vector relative to the rotating atmosphere; C_D is the coefficient of drag; A is the exposed cross-sectional area; m is the object's mass; $\vec{\omega}_{\oplus}$ is the mean motion of the Earth's rotation; $\vec{r}$ is the object position vector in an Earth Centered Inertial reference frame [17]; and ρ is atmospheric density. Density is highly dynamic and depends on a number of factors, including solar cycle, diurnal cycle, geomagnetic activity, altitude, and latitude. The drag coefficient, mass, and area of the object are typically combined to form the ballistic coefficient ($\beta = \frac{C_D A}{m}$). C_D and A can vary as a function of time. For this work, C_D is computed using the force model of Sutton [12] with an accommodation coefficient of $\alpha = 0.93$. The cross-sectional area, A, is computed using a spacecraft body model and attitude information.

1.2 Neutral Density Modeling/Retrieval

The High Accuracy Satellite Drag Model (HASDM) is an example of an empirical approach to density estimation. HASDM estimates a time-series of thirteen spherical harmonic global density and temperature correction coefficients using observations of 75-80 carefully selected calibration satellites (payloads and debris objects) in a batch fit [1], [2], [11]. Intensive sensor tasking is made available for this effort, which allows for the collection of approximately 500 observations per day per calibration satellite. HASDM decouples the ballistic coefficient and the density parameter by first solving for the long-term averaged ballistic coefficient of each satellite, averaging almost 3200 previously estimated values for each calibration satellite [2].

More recently, density modeling and forecasting methods have been developed that take advantage of physics-based models. For example, Sutton, et. al. [15] uses POD information of three Spire CubeSats to retrieve the effective energy dissipation rate (EDR) with a resolution of one orbital period. He then uses the EDRs to estimate driver parameters (most recent daily F10.7 and a 6-hour Kp index) to a physics-based model, TIE-GCM.

Our tool is named SoleiTool to emphasize its focus on the sun-driven nature of the near-Earth space environment. It also takes advantage of a physics-based model, while leveraging CubeSat GPS information to estimate TIE-GCM forcing parameters, specifically the Kp index while keeping a fixed F10.7. Kp describes geomagnetic activity which is typically driven by coronal mass ejections and high-speed solar wind, while F10.7 describes solar activity which is driven by the solar rotation and 11-year solar cycle [4]. (A perturbed space environment can be caused by either geomagnetic activity or solar activity.) The estimated Kp and fixed F10.7 indices are then input to TIE-GCM to obtain a predicted time-series of global density, which could be used in near real-time for satellite mission support or for atmospheric density predictions.

The specifics of our density estimation method are introduced in Section 2. Section 2.2.1 describes the three PF approaches that are the focus of evaluation in this work. The Spire CubeSat data used for assimilation are described

in Section 3. Section 4 provides a description of TIE-GCM and our unique approach to running it in such a way that vastly reduces filter computation time. Section 5 describes the case study and filter initializations. In Section 6, we analyze the performance of SoleiTool when applied to this case study for each of the three PF approaches. We conclude with a summary of findings and plans for future work.

2. METHOD

As shown in Fig. 1, SoleiTool is comprised of two filters. We have made various modifications to SoleiTool since first considering its use with debris object tracking data. Specifically, the first filter, originally an Unscented Kalman Filter, has been replaced with a Batch filter. The Batch filter ingests CubeSat POD measurements (described in detail in Section 3) and estimates a density coefficient (C_ρ) for a single arc of data. These inferred density coefficient measurements are passed to the PF to estimate a time-series of Kp with a fixed F10.7. Details on each filter are provided in Sections 2.1 and 2.2. The filter type, measurements, and estimated states of both filters are summarized in Table 1. Features of the Batch and PF design and implementation decisions have been informed by Spire data, TIE-GCM characteristics, and the case study.

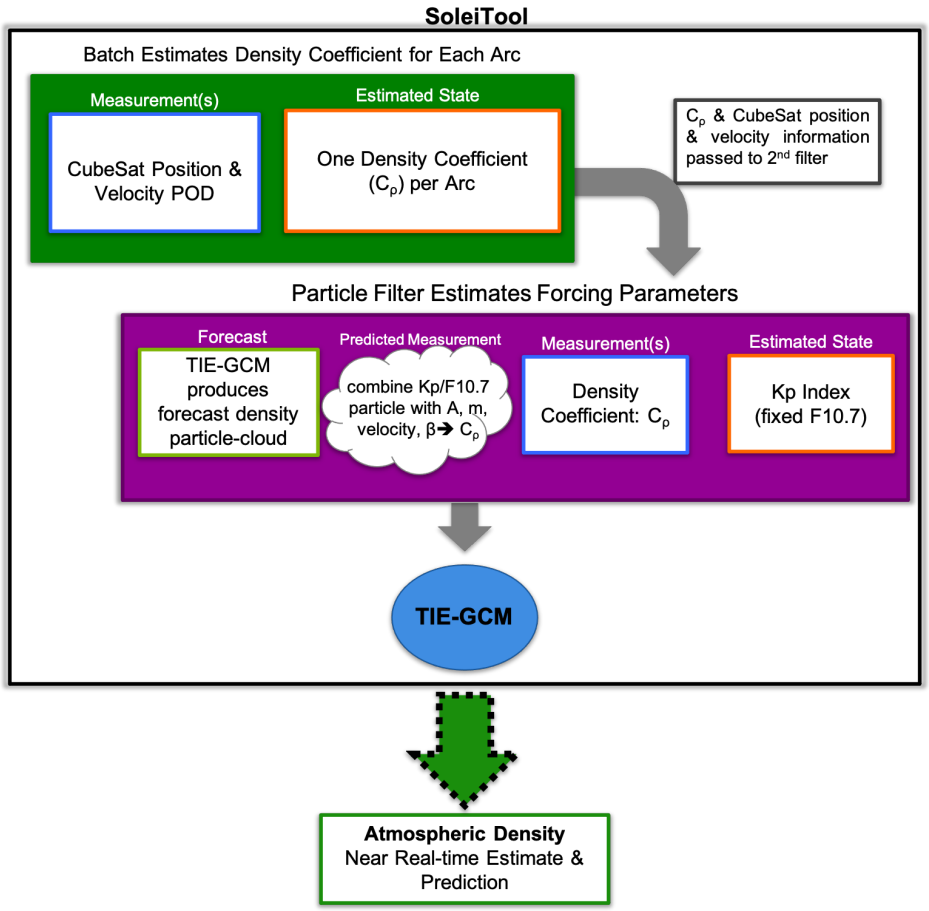

Fig. 1: SoleiTool Flow

Table 1: SoleiTool Batch and PF Summary

Filter Type	**Measurements**	**Estimated State**
1. Batch	CubeSat Position & Velocity POD	CubeSat Position & Velocity, C_ρ per Arc
2. PF	C_ρ	Kp

2.1 Batch Filter

The purpose of the Batch filter is to compare and quantify differences between the observed spacecraft trajectory (POD) and a trajectory propagated using a background density model. The background density model is a fixed density field generated with TIE-GCM for relatively calm conditions (i.e., input parameters of Kp=3 and F10.7=150). Any differences between these trajectories indicate that the true underlying density field is different than that generated using Kp=3 and F10.7=150 in TIE-GCM, and is quantified via the estimated density coefficient (C_ρ).

Orekit [5] is used to model the underlying orbit dynamics, including 140 degree/order gravity, sun, moon, and Jupiter third body perturbations, solar radiation pressure, solid tides, ocean tides, relativity, and atmospheric drag. We have augmented the standard Orekit atmospheric drag model to utilize TIE-GCM density rather than a conventional underlying density model included with Orekit, such as Harris Priester [5].

The Batch filter ingests CubeSat POD measurements,

$$\vec{y} = \left[\vec{r}_{POD}{}^T, \vec{v}_{POD}{}^T\right]^T \tag{3}$$

and estimates a density coefficient (C_ρ),

$$a_{drag} = -\frac{1}{2}\left(C_\rho * \rho_b\right)\frac{C_D A}{m} v_{rel}^2 \frac{\vec{v}_{rel}}{|\vec{v}_{rel}|} \tag{4}$$

for a single arc. Eq. 4 is simply Eq. 2 with the addition of C_ρ multiplying the background density field:

$$C_\rho * \rho_b \tag{5}$$

An arc is defined as 20 to 60 minutes of continuous POD for a single CubeSat. The estimated density coefficient multiples the background density model (ρ_b). The background density model is generated using Kp=3 and F10.7=150. SoleiTool loops through the data and runs an instance of the batch on each arc of data until the end of the data set is reached.

An estimated density coefficient greater than one ($C_\rho > 1$) indicates that the satellite experienced an enhanced density field (i.e., a density field generated by Kp $>$ 3 and/or F10.7 $>$ 150 s.f.u.) on average throughout the arc compared to the background density model (generated using Kp=3 and F10.7=150). On the other hand, an estimated density coefficient less than one ($C_\rho < 1$) indicates the satellite experienced less acceleration due to drag than that produced by the background density model, meaning that the true density field is likely generated using Kp $<$ 3 and/or F10.7 $<$ 150 s.f.u.. On occasion, the Batch filter estimates a negative coefficient of density which would signify a non-physical density field. These negative density coefficient estimates are replaced by .001. Once the Batch filter has processed all available CubeSat data, the C_ρ estimates for each arc are passed to the PF.

2.2 Particle Filter

Next, information from all arcs and all CubeSats is combined to ultimately reveal time varying global density. This is accomplished via a PF. The PF uses the time-series of all C_ρ estimates resulting from all runs of the Batch, for all CubeSats, to estimate a time-series of TIE-GCM input parameters. This paper explores three different PF approaches for TIE-GCM input parameter estimation. The approaches are described in detail in Section 2.2.1.

TIE-GCM is run to populate the Kp state-space for the length of the case study before filter execution (described in more detail in Section 4). This drastically reduces filter computation time because TIE-GCM is not called at any point during filter execution.

Kp and F10.7 are the primary drivers of TIE-GCM. Historically, F10.7 is less dynamic and remains relatively constant for days to weeks in time because it is driven by the 25-day solar rotation and 11-year solar cycle. Therefore, we estimate only a Kp time-series while holding F10.7 stationary. When SoleiTool is executed in near real-time, a fixed F10.7 can be chosen that is representative of the most recent several days of measured F10.7.

The PF applies corrections in the form of weight adjustments to the cloud of Kp particles based on the difference between the C_ρ predicted measurement and the C_ρ measurements (Batch filter estimates). The predicted C_ρ measurement for a particular Kp particle is the ratio between the Kp particle density ($\rho_{particle}$) and the background model density (at the satellite location and time of the C_ρ measurement), ρ_b:

$$C_{\rho\ predicted} = \frac{\rho_{particle}}{\rho_b} \tag{6}$$

After obtaining the time-series of Kp estimates, a smoother is applied in order to compute average Kp estimated over an hour. The smoother progresses forward in time at 15-minute increments; therefore, computing a smoothed Kp estimate every 15-minutes using one hour of Kp PF estimates.

The estimated, smoothed Kp time-series and fixed F10.7 are then input to TIE-GCM to produce a global density field that aims to capture the true underlying density field. It is noted that the density field does not typically react at the same rate as the measured Kp; the density field takes about a half day to fully respond to the energy input from an elevated Kp (geomagnetic storm). We do not aim to estimate the actual 3-hour global index of geomagnetic activity (Kp), but rather TIE-GCM input parameters that reproduce the observed CubeSat acceleration due to drag.

2.2.1 PF Approaches

Approach 1 estimates one Kp per C_ρ measurement and then a smoother is applied to obtain an average Kp for an hour of measurements, sliding forward in 15-minute increments. Instead of using only one C_ρ measurement to update the Kp state, the second PF approach combines information from an hour of C_ρ measurements to execute a state update. Therefore, information from various satellites at their locations can be applied to more effectively update the spread of PF particles to estimate a Kp representative of the global density field. Due to the nature of this approach, a smoother is not necessary; this approach should inherently provide less noisy Kp estimates and create a Kp index time-resolution of 1 hour.

Geomagnetic energy enters the polar regions before being transported to the equator, causing a more rapid density field enhancement in the polar regions. So, in Approach 3, we estimate a low and high latitude Kp to determine if the polar density field responds faster to the geomagnetic storm than the low latitude region ($<$ 60 deg. latitude). This approach builds upon Approach 2, so it also uses one-hour batched measurements.

The three approaches are listed below for reference:

- **Approach 1:** Fixed F10.7, Smoothing of results over time
- **Approach 2:** 1-Hour Batched Measurements & Fixed F10.7, 1 Kp per hour, Whole globe
- **Approach 3:** Zonal & 1-Hour Batched Measurements & Fixed F10.7, 2 Kp estimates per hour

3. SPIRE DATA

Spire Global has a growing 3U CubeSat constellation of 100+ CubeSats in the 400 to 600 km altitude range. Spire CubeSats carry dual-frequency GPS receivers that provide precise position information at 1Hz. GPS information is available for only portions of the orbit corresponding to the active duty cycle of each satellite. Depending on the satellite, the data collection portion of the orbits used here spans from 40 to 70 minutes. Ten minutes at the beginning and end of a continuous arc of POD is not used due to known POD solution degradation on POD edges. The remaining data, after trimming ten minutes at the beginning and end, is referred to hereafter as an arc of data. During the period of the 11-day case study, there are a total of 867 arcs for the nine CubeSats, combined; this results in 867 C_{rho} Batch estimates (one per arc) that are passed to the PF.

In this work, we assimilate Spire's Precision Orbit Determination (POD) ephemeris time-series. Spire logs and down-links GPS pseudorange and phase measurements, and produces ECEF POD using RTOrb [https://gps-solutions.com/brochures/GPSS_Brochure_RTOrb_ Nov_2011.pdf], a software that uses a Kalman filter-based approach to estimate orbit ephemeris. We transform ECEF POD to ECI using a standard, high-precision transformation in Orekit [5]. Spacecraft attitude information is also provided which is used to compute the CubeSat projected area facing into the velocity vector (A in Eq. 4), referred to as the projected area hereafter. Attitude information is only available during active arcs of data collection (when GPS information is available). Table 2 provides a description of the satellite orbits. Spire's internal satellite ID numbers are used to reference the satellites throughout this paper.

Table 2: Spire CubeSat Properties

Spire ID	NORAD ID	Lemur Version	Altitude (km)	Inclination	Mass (kg)
46	42779	3.0	480-510	SSO (LTDN 10:30)	4.45
62	43048	3.1	426-443	51.6 deg.	4.45
85	43558	3.3	472-484	51.6 deg.	4.93
86	43695	3.3	490-520	83 deg.	4.93
90	43745	3.3	460-510	SSO (LTDN 10:00)	4.93
99	44084	3.4	483-520	SSO (LTAN 09:30)	5.10
100	44085	3.4	483-520	SSO (LTAN 09:30)	5.10
101	44086	3.4	483-520	SSO (LTAN 09:30)	5.10
102	44087	3.4	483-520	SSO (LTAN 09:30)	5.10

Each satellite's mass and physical characteristics are known. The satellites used for this effort are one of four versions of the Lemur CubeSat; versions 3.0, 3.1, 3.3, and 3.4 of which 3.0 and 3.1 are physically equivalent. Table 2 identifies the Spire CubeSat version. Version 3.3 is bigger than version 3.1 by an inch (added to the total solar panel width on each side of spacecraft). Similarly, version 3.4 is bigger than version 3.3 because an additional solar panel is added to each side of the space craft body, making a total of 6 solar panels instead 4 (Fig. 2).

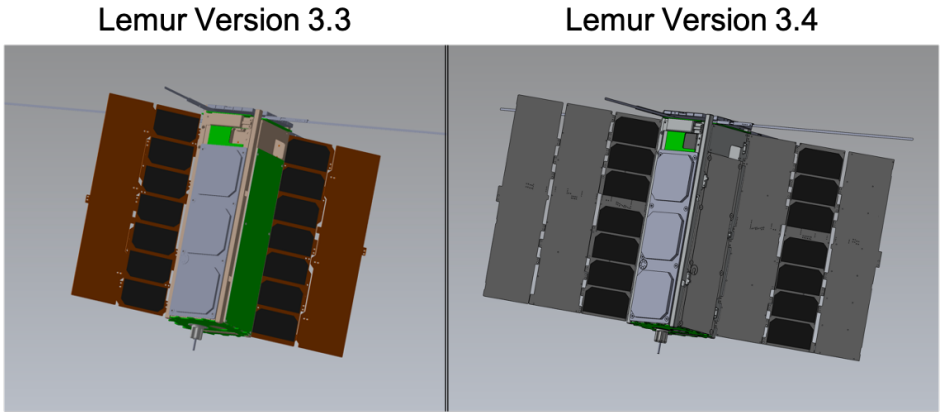

Fig. 2: Spire CubeSat Lemur Versions 3.3 and 3.4; Courtesy of Spire Global

4. TIE-GCM

TIE-GCM is an open source general circulation model developed by the National Center for Atmospheric Research (NCAR) [10]. It produces a three-dimensional, nonlinear representation of the coupled thermosphere and ionosphere system [13]. By adjusting its primary inputs, Kp and F10.7 indices, TIE-GCM can simulate global thermospheric mass density changes under various solar and geomagnetic activity levels. For the purpose of this work, the model output time step is set to 30 minutes and a default horizontal resolution of 5 degrees latitude and 5 degrees longitude is used, with a vertical pressure level size of a half-scale height, extending from about 97 to 500 or 700 km (depending on solar cycle/F10.7) [6].

Vertical interpolation is performed during post-processing of the model output to obtain atmospheric density at any LEO orbit altitude. During calm conditions (Kp $<$ 3 and F10.7 $<$ 150 solar flux units), the TIE-GCM does not reach LEO altitudes above about 500km. So, when it becomes necessary to obtain density values for calm conditions at higher altitudes in the PF, we fill-in any gaps in the TIE-GCM density model with the (Mass Spectrometer and Incoherent Scatter) Atmospheric Model [Picone, et al., 2002]. For the purpose of this work, all TIE-GCM runs are completed before filter execution. TIE-GCM is run to populate the Kp-F10.7 state-space (0 to 9 Kp and 67 to 273 F10.7) with a resolution of roughly .5 Kp and 15 s.f.u for F10.7 for the span of the case study dates.

In SoleiTool, the TIE-GCM runs to populate the Kp-F10.7 state-space for the length of the case study are run with steady-state Kp and F10.7. In other words, one run of TIE-GCM maintains a constant Kp and F10.7 value for the entirety of the case study. Therefore, when a density value for a particular Kp and F10.7 (at a particular time and location) is desired, the density value can be retrieved from a density database populated via previously executed TIE-GCM runs.

5. CASE STUDY

We demonstrate SoleiTool's ability to track the dynamical behavior of the space environment by evaluating its performance in a case study using CubeSat POD measurements collected during an 11-day time period in which two geomagnetic storms occur.

The case study covers May 10 - 21, 2019. This date range is selected because minor (Kp = 5) and moderate (Kp = 6) geomagnetic storms occurred on May 10 - 11 and 14, respectively (Fig. 3) [8]. Typically, a quiet or calm space environment is described as having both a relatively low Kp (Kp $\leq$ 2) and F10.7 (F10.7 $\leq$ 80) [16]. The measured F10.7 remains around 80 s.f.u. during this period of time (solar minimum), with some small variability, so a fixed F10.7 of 80 s.f.u. is chosen for the PF portion of SoleiTool.

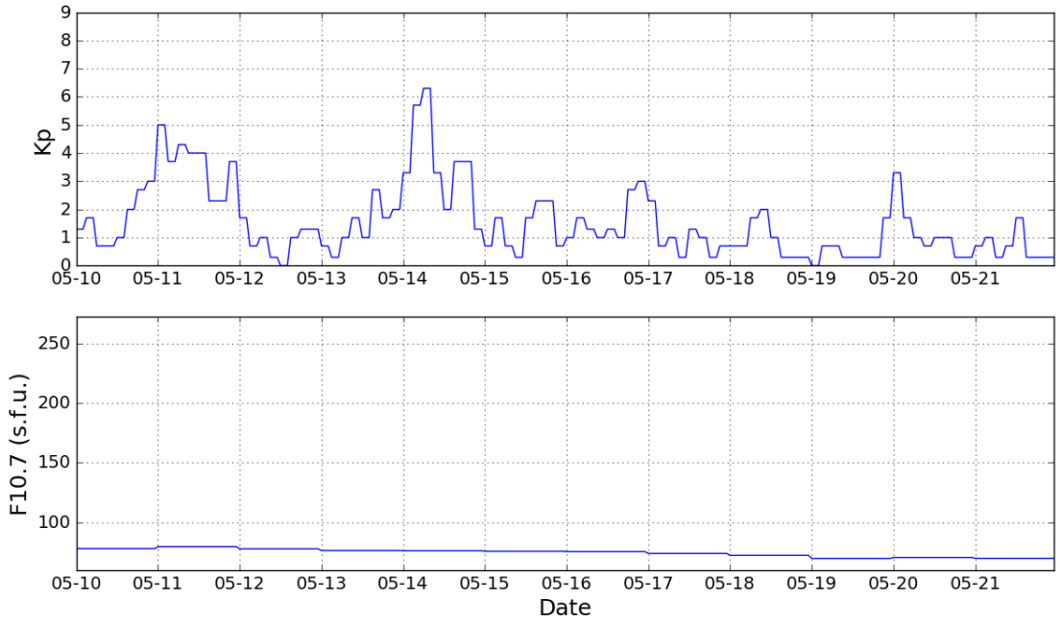

Fig. 3: Historical Kp and F10.7 for May 10- 21, 2019

5.1 Filter Initialization Details

The measurement variances for the POD position and velocity measurements are set to $\sigma^2 = (3m)^2$ and $\sigma = (1e\text{-}4m/s)^2$, respectively. The Batch filter estimated state is

$$\vec{X} = \left[\vec{r}^{\,T},\ \vec{v}^{\,T},\ C_\rho\right]^T \tag{7}$$

The initial $\vec{r}$ and $\vec{v}$ estimates are set to the first POD measurements reported for each arc. The initial C_ρ state is set to 1, meaning that a density field generated by the reference values of Kp=3 and F10.7=150 is assumed. An estimated C_ρ with a value other than one implies a density field other than that generated by the reference values in TIE-GCM. The initial Batch state covariance is set to

$$P_0 = diag\left(\left[(10m)^2, (10m)^2, (10m)^2, (0.1m/s)^2, (0.1m/s)^2, (0.1m/s)^2, (1)^2\right]\right) \tag{8}$$

In the second filter, the PF, the initial state estimate is set to

$$\vec{X}_0 = [Kp] = [1.5] \tag{9}$$

with a fixed F10.7 of 80 s.f.u. Note that the true Kp is unknown, so the initial state estimate is set to a Kp that represents calm conditions. The initial state covariance is

$$P_0 = \left[(1)^2\right] \tag{10}$$

An initial cloud of 50 Kp particles (χ_0) is generated via a normal distribution defined by the initial state (Eq. 9) and its *a priori* statistical information (10). The PF Kp state is estimated using "measurements" of C_ρ produced by the Batch filter (of all satellites combined). The results from the Batch and PF are presented separately in Sections 6.1 and 6.2, followed by the final estimated density of SoleiTool in Section 6.3.

6. RESULTS AND DISCUSSION

This section provides the Batch, PF, and overall SoleiTool results. First, the Batch results are discussed in the section below (Section 6.1). Then, the three PF approaches are analyzed via the estimated Kp time-series in plot form (Section 6.2). In Section 6.3, the three approaches are further investigated via the SoleiTool estimated density (TIE-GCM output using estimated Kp and fixed F10.7 input parameters) along a satellite trajectory. Lastly, a comparison between satellite POD and the propagated trajectory of a particular satellite using SoleiTool, MSIS, and HASDM is presented in Section 6.4.

6.1 Batch Filter

The Batch uses each arc of CubeSat POD measurements to estimate an independent density coefficient (Eq. 4). For satellite 62, a total of 84 arcs are used to estimate 84 density coefficients.The time-series of estimated density coefficients for satellite 62 is provided in Fig. 4a and the corresponding density, $C_\rho * \rho_b$, is shown in 4b. As expected, there is not a clear trend revealed by the estimated density coefficient, alone. The estimate density along this satellite's trajectory (Single-Satellite-Solution) indicates two geomagnetic storms. Fig. 4b also provides the HASDM density in gray. The historical Kp index is provided with each plot for reference of measured geomagnetic storms.

As mentioned in Section 2.1, the Batch filter estimates a negative coefficient of density on occasion, which are replaced replaced by .001 before being passed to the PF. These negative estimates are shown in the estimated density coefficient plots (Figures 4 and 5). Any large negative C_{rho} estimates are considered outliers and are removed from the dataset; here, satellite 62 has had one large negative C_{rho} outlier removed. The estimated density plots provide the density computed using corrected density coefficients (negative C_ρ estimates replaced with .001).

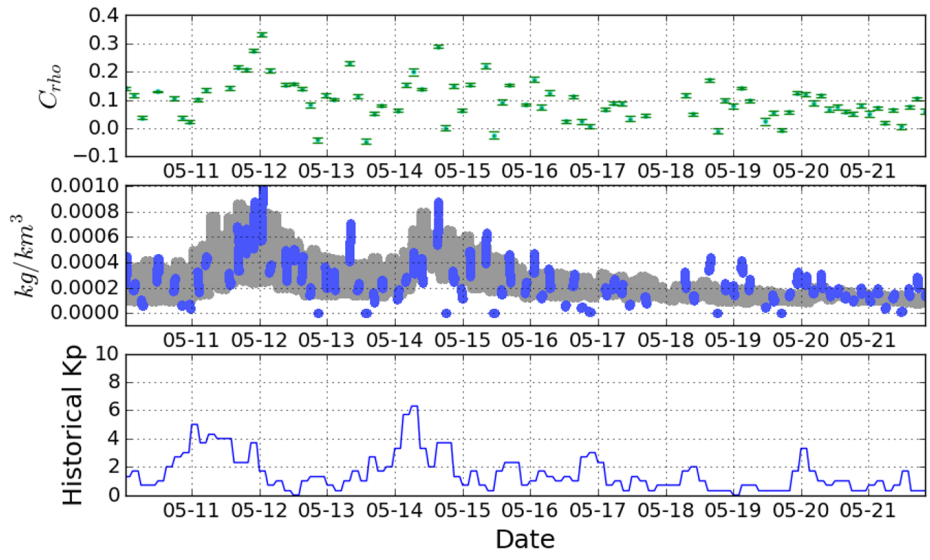

Fig. 4: Satellite 62 Batch Estimated Density Coefficient and its 3-σ Bounds; Batch Single-Satellite-Solution Density and HASDM Density (gray); Historical Measured Kp Index

Similar to satellite 62, the Batch results for satellite 99 are provided in Fig. 5. Satellite 99 is Lemur version 3.4 compared to version 3.1 for satellite 62. Therefore, satellite 99 has an additional solar panel on each side of the CubeSat body which could potentially lead to it being more sensitive to fluctuations in atmospheric density. However, this effect is likely canceled out due to satellite 99 orbiting about 60km higher than satellite 62. Satellite 99 has had four C_{rho} outliers removed.

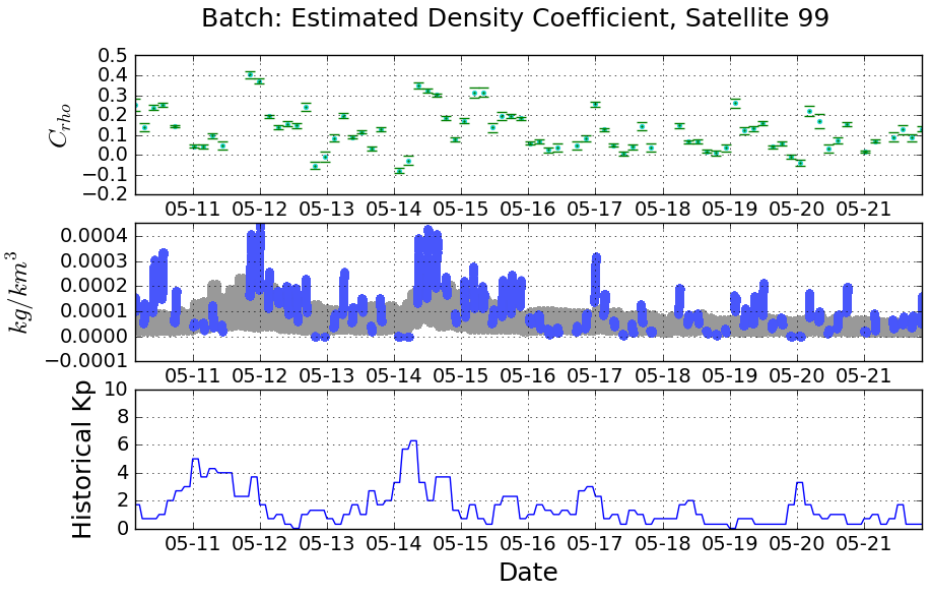

Fig. 5: Satellite 99 Batch Estimated Density Coefficient and its 3-σ Bounds; Batch Single-Satellite-Solution Density and HASDM Density (gray); Historical Measured Kp Index

The Batch estimated density coefficients for all satellites are passed as measurements to the PF.

6.2 Particle Filter

The PF accepts the C_ρ estimates from each CubeSat processed in the Batch filter and uses them as measurements to estimate a Kp. The three PF Approaches are summarized here for convenience:

- **Approach 1:** Fixed F10.7, Smoothing of results over time
- **Approach 2:** 1-Hour Batched Measurements & Fixed F10.7, 1 Kp per hour, Whole globe
- **Approach 3:** Zonal & 1-Hour Batched Measurements & Fixed F10.7, 2 Kp estimates per hour

The initial SoleiTool method was to estimate both Kp and F10.7 indices (using 100 particles). However, when this is done, the PF does not estimate a Kp and F10.7 time-series that is representative of the physical drivers of the density enhancement. Fig. 6 shows the PF Approach 0 estimated Kp and F10.7 time-series. The Kp and F10.7 retrievals in the PF are attributing more to F10.7 and less to Kp than one would expect from the historical record, where F10.7 is flat and Kp is quite elevated during the storms. Although this Kp and F10.7 is not reflective of the historical values, it may produce a density field that aligns with the truth. However, in order for TIE-GCM to be driven by the appropriate physics so that it can provide a density forecast, it is necessary to correctly attribute the physical drivers of a disturbed density field. We turn our attention to a fixed F10.7 (Approaches 1-3) for the remainder of this paper.

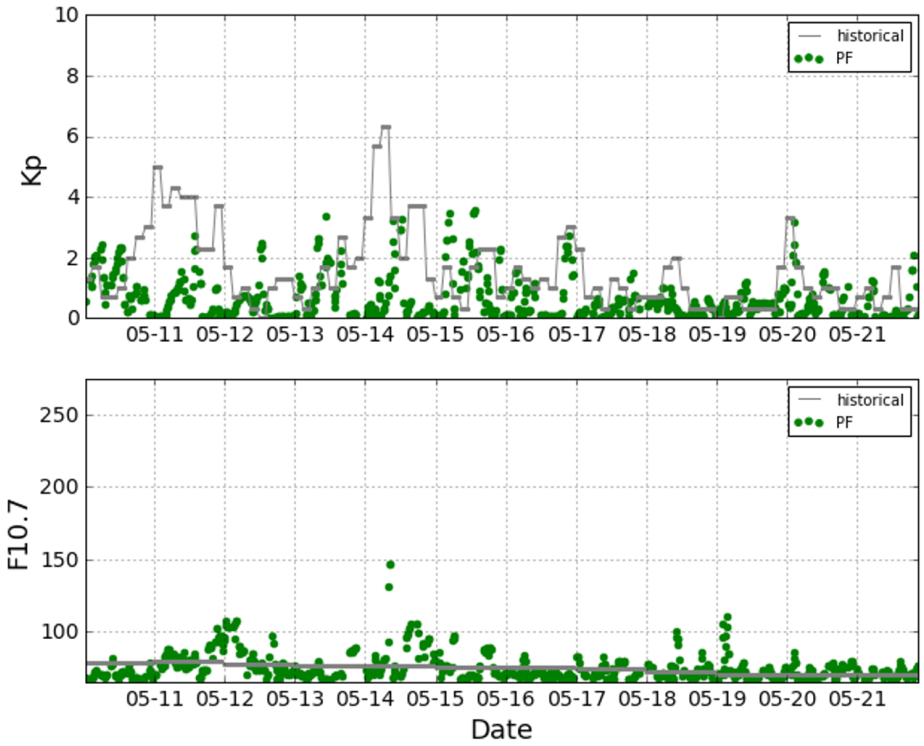

Fig. 6: **Approach 0:** Estimated Kp and F10.7 Time-series with Historically Measured Indices for Reference

Fig. 7 shows the estimated Kp from PF Approach 1 (fixed F10.7). The estimated Kp time-series is less noisy than PF Approach 0, and two Kp peaks occurring near the two geomagnetic storms can be seen. This result is more consistent with the observed behavior of these indices: more dynamic Kp, while keeping a relatively constant F10.7. Table 3 provides the average 3-σ Kp for Approaches 1-3; Approach 1 has larger average 3-σ Kp than the other approaches.

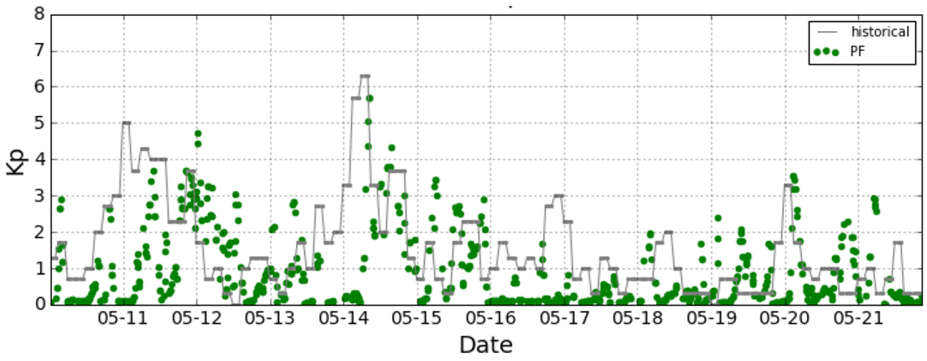

Fig. 7: **Approach 1:** Estimated Kp Time-series with Historically Measured Indices for Reference

To reduce the noise in the Kp estimates, we combine one hour of C_{rho} measurements to apply one Kp update in Approach 2. In Fig. 8, Approach 2 reveals a similar and slightly less noisy Kp time-series than Approach 1. Also, Approach 2 is a solution with lower uncertainty; the mean 3-σ Kp bound is 2.3, compared to 3.0 for Approach 1 (Table 3).

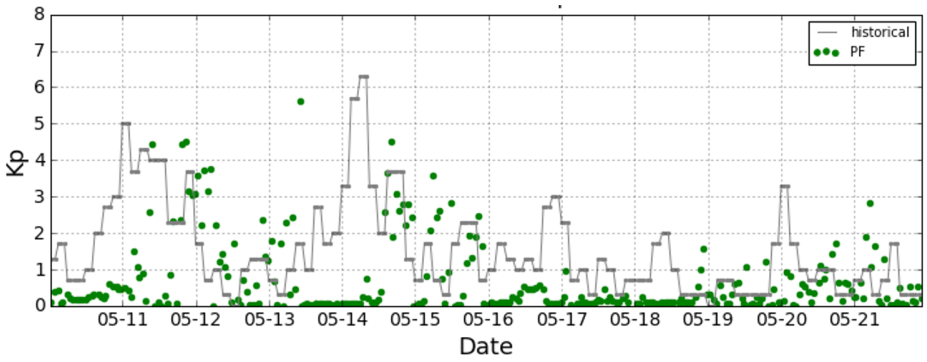

Fig. 8: **Approach 2:** Estimated Kp Time-series with Historically Measured Indices for Reference

Finally, recognizing that there may be different behavior at low and high latitudes, Kp is estimated for low (<60 deg.) and high latitude regions, separately. As expected, Fig. 9 shows that the high latitude Kp responds faster to the measured onset of the geomagnetic storms (historical indices). For example, in Fig. 9, an increase in the historical Kp index is measured beginning mid-way through May 10, 2019, and SoleiTool estimates an enhanced density field (represented via increased Kp index) in the high latitude regions almost immediately (mid-way through May 10, 2019). This is in contrast with the low latitude region, where SoleiTool does not sense an increase in density until mid-way through May 11, 2019. We note that a total of 654 C_{rho} measurements were used for low latitude Kp estimation, and only 213 for high latitudes. As shown in Table 3, Approach 3 has the lowest mean 3-σ Kp of all the approaches.

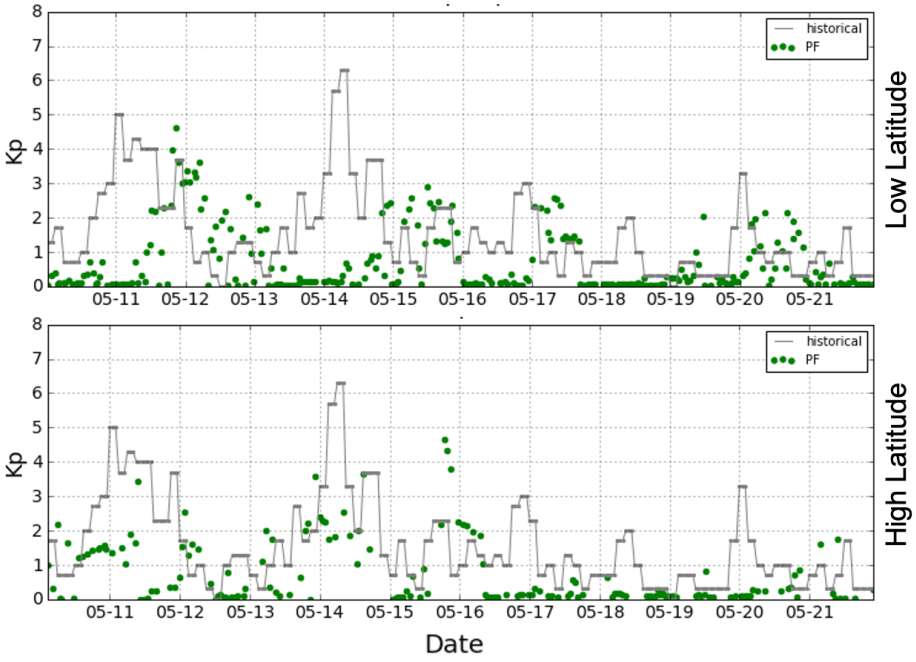

Fig. 9: **Approach 3:** Estimated Kp Time-series with Historically Measured Indices for Reference

Table 3: Average 3-σ Kp Bound for Each PF Approach

Index	Approach 1	Approach 2	Approach 3
Global Kp 3-σ	3.0	2.3	—
Low Latitude Kp 3-σ	—	—	1.9
High Latitude Kp 3-σ	—	—	2.2

In Section 6.3, we utilize SoleiTool's estimated Kp and F10.7 time-series as input parameters to TIE-GCM to obtain the estimated density along a particular satellite's trajectory.

6.3 SoleiTool Density

SoleiTool's final estimated density is obtained by using the estimated Kp and fixed F10.7 time-series as input to TIE-GCM. The *a priori* TIE-GCM runs described in Section 4 are again utilized here for computational efficiency. The SoleiTool estimated density along the trajectory of satellite 62 is provided in Figures 10-12 for Approaches 1-3. These figures also show the Batch single-satellite-solution estimated density (Eq. 5, computed using only satellite 62's POD), MSIS, and HASDM density for comparison. MSIS density is generated using the historical Kp and F10.7 indices. The top three plots (Batch, HASDM, and MSIS) remain the same for Approaches 1-3 (Figures 10-12).

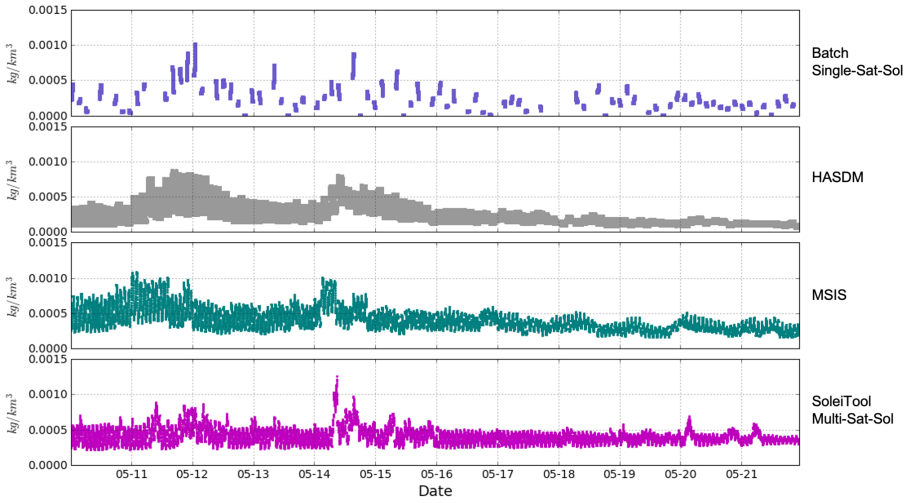

Fig. 10: **Approach 1:** Batch & SoleiTool Estimated Density Along Satellite 62 Trajectory Compared to MSIS and HASDM

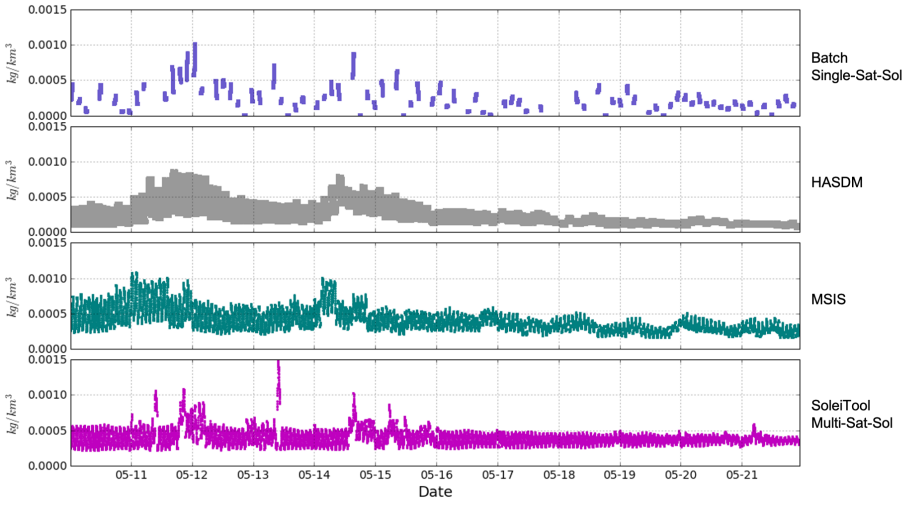

Fig. 11: **Approach 2:** Batch & SoleiTool Estimated Density Along Satellite 62 Trajectory Compared to MSIS and HASDM

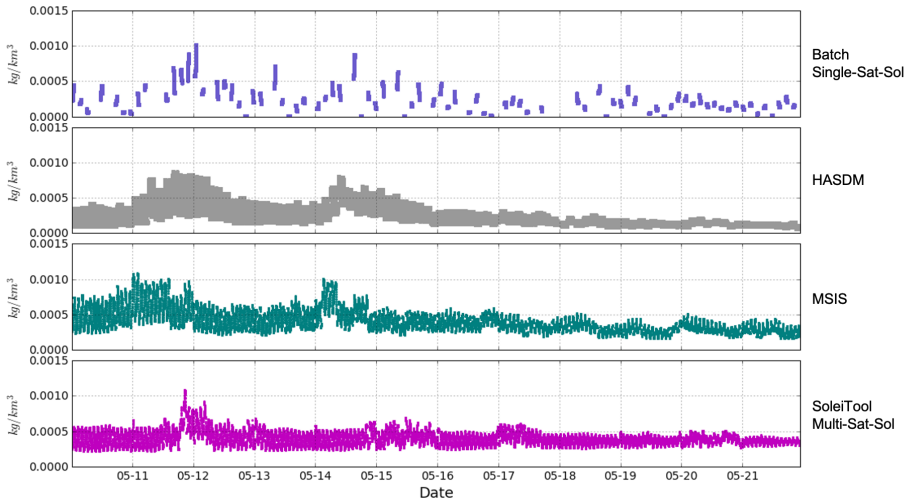

Fig. 12: **Approach 3:** Batch & SoleiTool Estimated Density Along Satellite 62 Trajectory Compared to MSIS and HASDM

In Approaches 1 and 2, the Batch, HASDM, and SoleiTool enhanced densities occur at relatively the same time. This is not the case for MSIS density because it is generated using historical Kp and F10.7, and historical Kp index has a measured peak earlier than the density field response. On the other hand, the second storm peak in Approach 3 appears to be both diluted and delayed compared to Batch and HASDM density. This could be caused in part by the number of measurements available to estimate the low latitude Kp; even though one hour of measurements are combined for each zone, there are fewer measurements available for each Kp update because the measurements have been split between two zones (high and low latitude regions).

Similarly, Approaches 1 and 2 have outlier high density features along the satellite 62 trajectory for the span of only about an hour (on May 14th for Approach 1, on May 13th for Approach 2). We notice that these outlier features do not occur in Approach 3 for satellite 62. It requires further investigation to determine the cause of this, but it could be be due to measurements being split up between the low and high latitude regions and, therefore, not having as much of an impact on the state when not combined.

One of the strengths of SoleiTool when compared to what is used operationally, is the time resolution. SoleiTool provides updated TIE-GCM input parameter(s) with a time resolution of 1 hour. Whereas, HASDM has a 3-hour time resolution. Because of this, we are able to discover finer time-scale features as the ones discussed earlier. These features may be due to one or two satellites that pass through a region of high density, but this region of high density is not representative of what is occurring on a global scale. This, as mentioned before, is one of the reasons we applied a Zonal PF to this case study. A spherical harmonic PF may be the best route moving forward to identify and represent these smaller-region features, but there is not enough satellite data in this case study to support such an approach.

6.4 Satellite Propagation Analysis

The desired end result of SoleiTool is improved atmospheric density modeling to allow for more accurate LEO object trajectory prediction. To evaluate this, satellite 62 is propagated with SoleiTool (Approaches 1-3), MSIS, and HASDM. The propagated trajectory for each is then compared to satellite 62 POD to obtain the overall trajectory difference magnitude at the end of the propagated arc. The trajectory is propagated for a 35-minute arc due to the characteristics of the POD it is being compared to: GPS duty cycle and solution degradation on POD edges (discussed in Section 3). Because the behavior of density is extremely dynamic during a geomagnetic storm, we analyze each model's propagation performance at the beginning (mid-day May 11), peak (beginning of May 12), and end (mid-day May 12) of the first storm. Table 4 provides the model propagated trajectory difference with the POD at the end of each 35-minute arc. All propagated trajectories have inherent error that is not due to density, but another unknown dynamical effect. So, there is always a baseline error; of which, the error due to density accumulates on. Each trajectory, for SoleiTool, MSIS, and HASDM, is propagated using the same dynamical models in Orekit; the only difference is the underlying density model.

Table 4: Model Trajectory Propagation Performance Comparison between SoleiTool Approach 1-3, MSIS, & HASDM

Model	Storm Beginning (m)	Storm Peak (m)	Storm End (m)
SoleiTool Approach 1	0.4	3.1	0.9
SoleiTool Approach 2	0.4	2.6	0.8
SoleiTool Approach 3	0.3	2.4	0.8
MSIS	2.7	2.4	1.2
HASDM	0.5	2.0	0.3

The values in Table 4 should be compared each column, separately. For example, column 1 provides each model's propagation performance at the beginning of the first storm. In all cases, Approach 3 has the best performance of the SoleiTool approaches. SoleiTool Approach 3 outperforms HASDM in the beginning of the storm. While, HASDM only outperforms SoleiTool by 0.4 meters during storm peak. At the end of the storm, all the SoleiTool approaches have similar performance and are outperformed by HASDM.

7. CONCLUSION AND FUTURE WORK

We have demonstrated SoleiTool's ability to utilize CubeSat POD information from nine satellites to estimate atmospheric density. First, we provided the Batch Single-Satellite-Solution in which it uses an arc of POD information from a single satellite to estimate a density coefficient that informs the space environment the satellite is traversing through. The Batch portion of SoleiTool processes each CubeSat POD data for the length of the case study to extract space environment information via density coefficient estimation for each arc. This information for all CubeSats is combined and passed to the PF to estimate the Kp index. The performance of each of the three PF Approaches were evaluated in the following ways: analysis of the estimated Kp time-series and its mean 3-σ bounds, comparison of SoleiTool estimated density with HASDM and MSIS, and CubeSat location difference with POD after propagating the trajectory for 35 minutes with SoleiTool, HASDM, and MSIS density.

We found that Approach 3 had the least noisy Kp estimates and also the highest confidence in the solution, which was demonstrated via the lowest average 3-σ Kp bound (Table 3). Approach 3 also showed that the polar regions do indeed become enhanced faster than other regions (as shown via a comparison to the low latitude region Kp estimates in Fig. 9). For the direct comparison between SoleiTool estimated density and HASDM/MSIS density, it was found that even though SoleiTool is using only nine CubeSats it is still able to align relatively well with HASDM. Approaches 1 and 2 estimate storms of similar magnitude with peaks at the same time as HASDM. Approach 3 density along satellite 62 trajectory did not perform as well at identifying the second storm and this is likely due to measurements being split between zones, so less information is available per zone.

The purpose of SoleiTool is to improve atmospheric density estimates in order to allow for more accurate LEO object motion prediction. Therefore, we compared how the propagation using SoleiTool density compares to propagation using HASDM and MSIS density. Approach 3 outperforms all other SoleiTool approaches in all cases. SoleiTool outperforms HASDM at the beginning of the storms and aligns well with HASDM at storm peak (0.4-meter difference). HASDM outperforms SoleiTool by a larger amount for the end of the storm.

Ultimately, Approach 3 seems to be the best approach. It has the most certain (lowest average 3-σ Kp bound) and least noisy Kp solution, while also outperforming all other SoleiTool approaches in trajectory propagation. Theoretically, Approach 3 builds upon Approaches 1 and 2, so it is understandable why it would outperform them. We believe that Approach 3, the Zonal PF, is the strongest approach, but requires more information (POD from larger number of CubeSats) in order to demonstrate its true capability.

Overall, this case study allows us to evaluate SoleiTool's performance using nine CubeSats (ranging from 420-520km altitude) for 11 days to estimate a dynamical space environment. Whereas, the operationally used HASDM effort used 75-80 satellites ranging from 200-800km altitude. The true strength of our method is its potential to exploit data already collected on large LEO constellations. The end goal is a data assimilation framework that characterizes atmospheric density in near real-time by leveraging classes of objects not typically utilized: CubeSats. Our tool is expected to improve atmospheric density estimates, which will allow for more accurate LEO object motion prediction. In doing so, we hope to decrease the number of unnecessary satellite maneuvers executed to avoid debris objects. This

not only extends satellite lifetime, but also provides for a safer space environment by preserving fuel to correct for actual collision risks.

8. REFERENCES

[1] Bowman, B., Storz, M.F., 2002. Time Series Analysis of HASDM Thermospheric Temperature and Density Corrections. In: AIAA/AAS Astrodynamics Specialist Conference.

[2] Bowman, B., Storz, M.F., 2003. High accuracy satellite drag model (HASDM) review. *Advances in the Astronautical Sciences*. 116. 1943-1952.

[3] Bowman, B. R., Tobiska, W. K., Marcos, F. A., Huang, C. Y., Lin, C. S., Burke, W. J. 2008. A new empirical thermospheric density model JB2008 using new solar and geomagnetic indices. In AIAA/AAS Astrodynamics Specialist Conference and Exhibit, Honolulu, Hawaii.

[4] Kirov, B., Asenovski, S., Georgieva, K. et al. 2015. What causes geomagnetic activity during sunspot minimum? *Geomagn. Aeron.*. 1033?1038 (2015).

[5] Maisonobe, L., Lee, I.-T., Pommier, V., Parraud, P., 2010. Orekit: an open-source library for operational flight dynamics applications. In International conference on astrodynamics tool and techniques, pp. 3-6, 2010.

[6] Matsuo, T., Lee, I.-T., Anderson, J.L., 2013. Thermospheric mass density specification using an ensemble Kalman filter. *Journal of Geophysical Research*. Space Physics. 118. 1339-1350. 10.1002/jgra.50162.

[7] Mutschler, S., P. Axelrad, T. Matsuo, E. Sutton, 2019. Physics-based Approach to Density Estimation and Prediction using Orbital Debris Tracking Data. Proceedings of the Advanced Maui Optical and Space Surveillance Technologies Conference, Maui, HI, 11 pages, September 17-20.

[8] NOAA Space Weather Scales, 2011. Space Weather Prediction Center www.swpc.noaa.gov/noaa-scales-explanation (accessed 6.20.20).

[9] Picone, J. M., Hedin, A. E., Drob, D. P., Aikin, A. C., 2002. NRLMSISE- 00 Empirical Model of the Atmosphere: Statistical Comparisons and Scientific Issues. Journal of Geophysical Research. 107 (A12), 1468.

[10] Qian, L., et al. (2014), The NCAR TIE-GCM: A community model of the coupled thermosphere/ionosphere system. In: *Modeling the Ionosphere-Thermosphere*. Geophysical Monograph Series, vol. 201, edited by J. D. Huba, pages 73-83., AGU, Washington, D. C, doi: 10.1002/9781118704417.ch7.

[11] Storz, M.F., Bowman, B.R., Branson, J.I., Casali, S.J., Tobiska, W.K., 2005. High Accuracy Satellite Drag Model (HASDM). *Advances in Space Research*, 36 (12), 2497-2505.

[12] Sutton, E., 2012. Normalized force coefficients for satellites with elongated shapes. *Journal of Spacecraft and Rockets*. 46(1), 112-116.

[13] Sutton, E., Cable, S., Lin, C., Qian, L., Weimer, D.R., 2012. Thermospheric basis functions for improved dynamic calibration of semi-empirical models. *Space Weather*. 10. 10.1029/2012SW000827.

[14] Sutton, E., 2018. A New Method of Physics-Based Data Assimilation for the Quiet and Disturbed Thermosphere. *Space Weather*. 16 (6), 736-753.

[15] Sutton, E., Thayer, J., Pilinski, M., Mutschler, S. Berger, T., Nguyen, V., Masters, D. 2021. Toward Accurate Physics-Based Specifications of Neutral Density using GNSS-Enabled Small Satellites. *Space Weather*. 10.1029/2021SW002736, 2021. 1.

[16] Thompson, R., Space Weather Indices, Australian Government Bureau of Meteorology www.sws.bom.gov.au/Educational/1/2/4 (accessed 6.20.20)

[17] Vallado, D.A., 2013. *Fundamentals of Astrodynamics and Applications*. Space Technology Library.